Bio-inspired dental multilayers: Effects of layer architecture on the contact-induced deformation ☆

J. Du [a,b], X. Niu [c], N. Rahbar [d], W. Soboyejo [a,b,e],*

[a] Department of Mechanical and Aerospace Engineering, Engineering Quadrangle Room D404B, Princeton University, Princeton, NJ 08544, USA
[b] The Princeton Institute for the Science and Technology of Materials (PRISM), Princeton University, Princeton, NJ 08544, USA
[c] Department of Mechanical and Biomedical Engineering, City University of Hong Kong, Kowloon, Hong Kong
[d] Department of Civil and Environmental Engineering, University of Massachusetts Dartmouth, North Dartmouth, MA 02747, USA
[e] Department of Materials Science and Engineering, African University of Science and Technology, Abuja, Federal Capital Territory, Nigeria

ARTICLE INFO

ABSTRACT

The ceramic crown structures under occlusal contact are idealized as flat multilayered structures that are deformed under Hertzian contact loading. Those multilayers consist of a crown-like ceramic top layer, an adhesive layer and the dentin-like substrate. Bio-inspired design of the adhesive layer proposed functionally graded multilayers (FGM) that mimic the dentin–enamel junction in natural teeth. This paper examines the effects of FGM layer architecture on the contact-induced deformation of bio-inspired dental multilayers. Finite element modeling was used to explore the effects of thickness and architecture on the contact-induced stresses that are induced in bio-inspired dental multilayers. A layered nanocomposite structure was then fabricated by the sequential rolling of micro-scale nanocomposite materials with local moduli that increase from the side near the soft dentin-like polymer composite foundation to the side near the top ceramic layer. The loading rate dependence of the critical failure loads is shown to be well predicted by a slow crack growth model, which integrates the actual mechanical properties that are obtained from nanoindentation experiments.

© 2012 Acta Materialia Inc. Published by Elsevier Ltd. All rights reserved.

1. Introduction

Dental crowns generate over $2 billion in revenue each year, with 20% of crowns being all-ceramic units [1]. However, they continue to fail at a rate of ~3% per year [2]. For some restorations in which ceramics are used as the top layer, more than 20% of them failed within the first 5 years of use [3]. This has stimulated research efforts to develop ceramic crowns that are more resistant to cracking under occlusal contact. In most cases, the ceramic crown structures are idealized as flat multilayered structures that are deformed under Hertzian contact loading [4]. This often leads to the pop-in of a subsurface radial crack due to the stress concentration in the subsurface regime in the top ceramic layer [5], which is consistent with the major clinical mode, as reported by Kelly [6].

The opportunity to reduce the stress concentrations (at the bottom of the top ceramic layer in crown structures) was inspired by the nanoindentation measurements of Marshall et al. [7], who showed that the Young's modulus varies from ~70 GPa for enamel to ~20 GPa for dentin. The variation in Young's modulus across the dentin–enamel junction (DEJ) was also shown to be approximately linear. Inspired by the DEJ structure and the linear gradation in the Young's modulus of the DEJ, Huang et al. [5] modeled the Hertzian contact-induced stress concentrations. Their results showed that the bio-inspired functionally graded structure resulted in lower stresses in the subsurface region of the top ceramic layer. Subsequent work by Niu et al. [8] and Rahbar et al. [9] also showed similar reductions in stress concentrations, which were later confirmed by the experimental work of Niu et al. [8].

In this paper, the design of the functionally graded multilayer (FGM) structure is optimized by simulating the effects of layer architecture by the finite element method (FEM). A processing method for the fabrication of bio-inspired, layered, nanocomposite FGM, is then presented. The variations in Young's modulus across the FGM are measured using nanoindentation techniques. The measured Young's moduli are then incorporated into a slow crack growth (SCG) model for the prediction of pop-in loads. The predictions of pop-in loads, at different loading rates, are validated on bio-inspired FGM.

2. Design of FGM structure

2.1. Design of FGM thickness

The finite element simulations were carried out using the Abaqus FEA software package (Dassault Systemes Simulia Corporation, Providence, RI) to model the stress distributions in the dental multilayers. The simulations considered idealizations of bio-inspired dental multilayers, as well as a single join layer of dental adhesive material. Axisymmetric geometries were used to simplify the problem, as shown in Fig. 1.

A 4-node linear axisymmetric quadrilateral element was used in the mesh. In an effort to capture the high stress concentration, the mesh was dense in the regions near the axisymmetric axis of the model. The bottom of the substrate was fixed, while the axisymmetric boundary condition was added on the axisymmetric axis. A load of 100 N was applied to the Hertzian indenter, which was modeled as a rigid surface. The materials and the properties used in the simulation are listed in Table 1.

The FGM was modeled as 10 sublayers, with equal layer thicknesses. The Young's modulus was increased linearly from 18 GPa in the foundation to 205 GPa in the top ceramic layer. Poisson's ratio was assumed to be 0.3 for all the materials. The geometry of the dental multilayered structure and the Hertzian indenter are presented in Fig. 1. The thickness of the bonding layer was modeled to be 100, 250, 500 and 1000 μm, respectively.

The maximum principal stress at the subsurface center of the top ceramic layer, which is associated with the major clinical failure mode, the subsurface radial crack [6], in the dental multilayer, is presented in Fig. 2. Fig. 3 shows the effects of layer thickness on the stress distribution in the dental multilayered structure, with and without FGM.

At each thickness, the maximum principal stress at the subsurface center of the top ceramic layer was always lower in the structures with FGM than in those without FGM. The stress concentrations in the structures with FGM were also less severe than those in the structures without FGM. Since the FGM had a larger overall Young's modulus, hence greater stiffness, than the single dental adhesive layer, under Hertzian contact loading, the top ceramic layer received better support from the stiffer FGM layer than from the single dental adhesive layer. Also, the stress inside the FGM was greater than that inside the single adhesive layer. This serves as a stress buffer to the top ceramic layer, when stress dissipates from the top ceramic layer into the FGM.
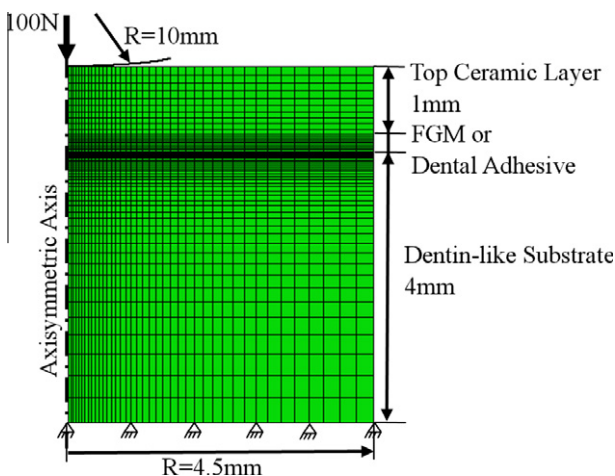

Fig. 1. FEM model of dental multilayer structure subjected to Hertzian contact loading.

Table 1
Material properties of dental materials.

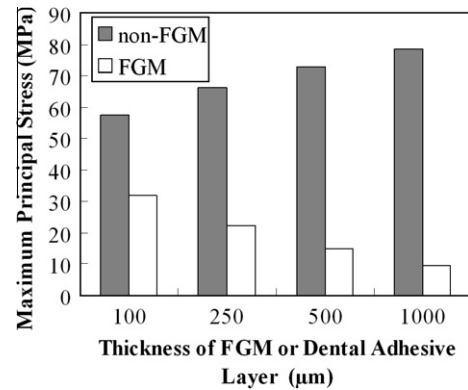| Layer	Material	Young's modulus (GPa)
Top ceramic layer	Zirconia	205
Dental adhesive layer	Rely X ARC	5
Substrate	Z100	18

Fig. 2. Maximum principal stresses in the subsurface region of the ceramic top layer with or without FGM for different adhesive layer thicknesses.

As the thickness of the FGM increases, the stress concentration in the structure is reduced, and the maximum principal stress in the subsurface center of the top ceramic layer decreases. Thicker FGM provide better support to the top ceramic layer, because it has higher stiffness. However, when the thickness of the single dental adhesive layer increases, the opposite is true.

2.2. Design of FGM architecture

This section presents the results of efforts to optimize the design of the FGM structure by conducting finite element simulations of the stress distribution in possible FGM structures. Finite element simulations were carried out using the same geometry and boundary conditions as shown in Fig. 1. The thickness of the FGM structures was fixed at 100 μm, while the Young's modulus distribution in the FGM was given by

$$E(x) = E_{substrate} + \left(\frac{x}{t}\right)^n (E_{top} - E_{substrate}) \tag{1a}$$

where x is the distance from the substrate, t is the thickness of the FGM, which in this case is 100 μm, and E_{top} and $E_{substrate}$ are the Young's moduli of the top ceramic layer and the substrate, respectively. Hence, the Young's modulus of the FGM varies from that of the substrate to that of the top layer. When the exponent n is small, the change is more dramatic near the substrate; when it is big, the opposite is true. When n equals 1, the distribution is linear. As a comparison, the sinusoidal distribution was also simulated, where

$$E(x) = E_{substrate} + \frac{1 - \cos(x\pi/t)}{2}(E_{top} - E_{substrate}) \tag{1b}$$

The variations in the Young's moduli are presented in Fig. 4 for the different types of modulus gradations.

The maximum principal stress at the subsurface center of the top ceramic layer and the maximum value of the maximum principal stress in the FGM are compared in Fig. 5. The sinusoidal distribution does not have particular advantages. Compared with the linear distribution, it generates similar stresses in the top ceramic layer, but much higher stresses in the FGM. For the power law distributions, when the exponent increases, the stiffness of the FGM
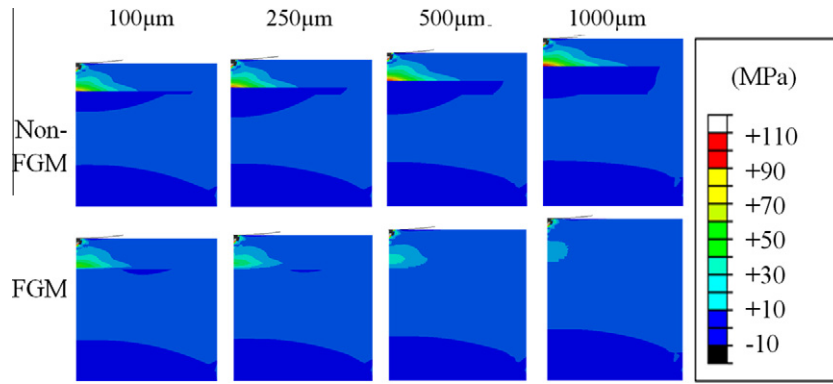
Fig. 3. Maximum principal stress distributions in the dental multilayer structures with or without FGM for different adhesive layer thicknesses.
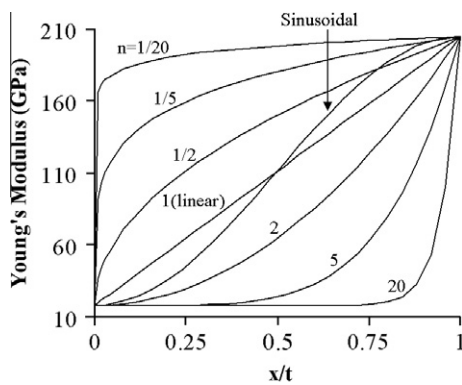

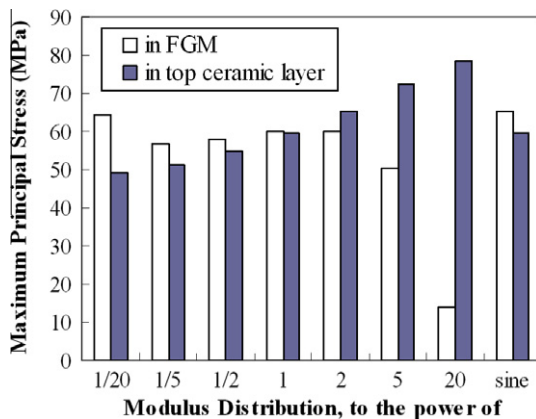**Fig. 4.** Distributions of Young's modulus in the FGM layer.

Fig. 5. Comparison of maximum principal stress inside the top ceramic layer and FGM layer with different distributions of Young's modulus.

decreases. Thus, the support it offers to the top ceramic layer decreases.

The stresses in the top ceramic layer increase with increasing exponent n. Furthermore, the overall stress levels in the FGM also decrease with increasing exponent, although the distribution of the stress was more uniform for smaller exponents n. The combined effect of the decreasing stress dissipated into the FGM and less uniform stress distribution with increasing exponent n gives the trend of the maximum value of the maximum principal stress in the FGM, as shown in Fig. 5.

If the fracture toughness of the FGM is greater than or comparable with that of the top ceramic layer, the power law distribution with an exponent equal to or smaller than 1/5 could be the most favorable design, since it lowers the stresses in the top ceramic layer. In contrast, if the FGM has lower fracture toughness than the ceramic layer, the power law distribution with an exponent $\geqslant 5$ might be favored. This is because, although the stresses in the ceramic layer increase, the FGM bears less stress. If the FGM has fracture toughness comparable with that of the ceramic, a linear distribution will be favored, since it results in comparable maximum stresses in the FGM and the top ceramic layer.

3. Fabrication and characterization of dental multilayers

3.1. Fabrication of dental multilayer using nanocomposite materials

A 4-mm-thick 10×10 cm (4×4 inch) steel plate mold (Fig. 6a) was used for the fabrication of the bio-inspired FGM structure. The plate contained four drilled holes that were sealed with Teflon rings, so that four samples could be fabricated at the same time. The holes had diameters of 9 mm. The substrate was a dentin-like soft material, Z100 restorative (3M ESPE Dental Products, St. Paul, MN), which is a clinically used dental material. They were molded in the holes and then cured with UV light for 40 s on both sides. The thickness of the fabricated Z100 substrate was ∼4 mm, the same as that of the steel plate mold.

The FGM were produced using nanocomposite materials, a mixture of zirconia or alumina nanoparticles (Nanotek Instrument Inc., Dayton, OH) and an epoxy matrix, EPO-TEK 301 (Epoxy Technology Inc., Billerica, MA). The nanoparticles had an average diameter of ∼20 nm. After mixing, the nanocomposite material was deposited onto the steel plate mold with the substrate staying in it. A wire-wound wet-film applicator rod (Gardco, Pompano Beach, FL) was then used to spread the nanocomposite material across the steel plate, as shown in Fig. 6b.

When pulled across the steel plate, with a fluid film in front of the rod, the applicators could control the volume per unit area and thus the thickness of the fluid film. Since the size scale of the rod thread was much greater than the diameter of the nanoparticles, the applicator rod did not strain them out of the composite.

After each layer had been deposited and spread, the plate was cured in a vacuum oven at 65 °C for 1 h. The deposition and curing process was then repeated to build up the multilayered structures. From bottom to top, the functionally graded nanocomposite layers contained 10 wt% zirconia, 20 wt% zirconia, . . ., 70 wt% zirconia, 40 wt% alumina and 45 wt% alumina, respectively. The variations in filler loading/type are intended to change the stiffness of the layers.

The crown-like dental ceramic layer on top was fabricated from a medical grade 3 mol.% yttria-stabilized zirconia rod (YTZP; Saint-
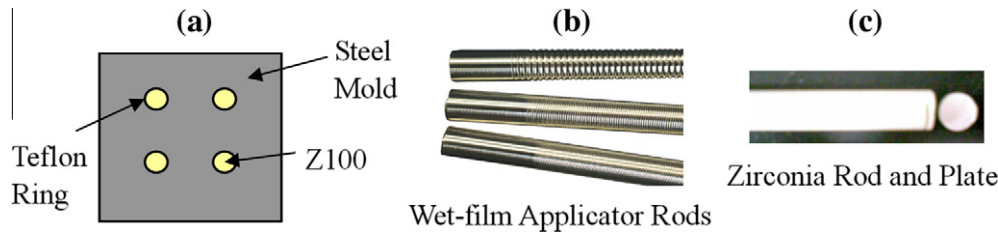
Fig. 6. Schematic of FGM structure fabrication processes.

Gobain, Colorado Springs, CO). It was sliced and polished into ~1-mm-thick plates, as shown in Fig. 6c. It was then pressed onto the last layer of the FGM before curing.

Finally, the multilayered structures ~9 mm in diameter and ~5 mm thick were cut and removed from the mold. They were then cleaned with distilled water and blow dried with compressed air.

3.2. Nanoindentation measurements

The fabricated multilayered structure was saw cut to produce a horizontal cross section. The cross sections were then ground and diamond polished. Nanoindentation measurements were then carried out on the polished cross sections to measure the variations in the Young's modulus from the top ceramic layer to the dentin-like foundation. The nanoindentation measurements were carried out with a TriboScope nanomechanical testing system (Hysitron Inc., Minneapolis, MN), coupled to a Dimension 3100 scanning probe microscope (Bruker AXS Inc., Madison, WI). A cube corner indenter tip was used. The loading profile consisted of the following three steps: loading in 5 s to a peak load of 3 mN, holding at the peak load for 15 s, and returning to zero load in another 5 s. To minimize the possible interactions between adjacent indents, all the indents were separated by at least 10 μm.

3.3. Hertzian contact experiments

Hertzian contact tests were performed on the fabricated dental multilayered structures. The tests were carried out in an Instron 8872 hydraulic mechanical tester (Instron, Canton, MA, USA). They were conducted in air at room temperature and a relative humidity of ~25%. The Hertzian contact tests were performed under load control with a hemispherical tungsten carbide loading probe with a diameter of 20 mm. The forces measured during mastication and swallowing were ~5–364 N. The maximum force recorded during clenching efforts could be 216–890 N [10]. Meanwhile, the average chewing rate is about one chew per second [11]. Therefore, the tests were performed at clinically relevant loading rates between 1 N s^{-1} and 1000 N s^{-1}. The loads and displacements were recorded by the tester. The critical loads were then determined as the loads at which discontinuities in displacement were observed. These were also found to correspond to the onset of cracking, which could be heard clearly during the tests.

3.4. SCG model

The SCG model suggests that, during contact damage in the dental multilayered structures, subsurface radial crack growth occurs solely as a result of SCG in the top ceramic layers [12–14]. For cases in which the initial crack length is very small, and the final crack length is much greater than the initial crack length, the radial crack propagation can be described by the standard power law SCG theory [12,15,16]. This gives

$$\int_0^{t_R} \sigma(t)^N dt = D \tag{2}$$

where t is the time, $\sigma(t)$ is the time-dependent expression of the stress state (pure tensile stress) that will introduce mode I cracks in the middle point of subsurface of top ceramic layer, and t_R is the rupture time at which subsurface radial cracks occur. When the loading rate $\dot{P}$ is constant, the rupture time t_R can be expressed as $t_R = P_c/\dot{P}$, where P_c is the critical load. The parameter D in Eq. (2) is a time- and load-independent quantity, given by [16]

$$D = \frac{K_{Ic}^N(c_0^{1-N/2} - c_f^{1-N/2})}{(N/2 - 1)v_0\beta^N} \tag{3}$$

where K_{Ic} is the fracture toughness, N is the crack velocity exponent, which in this case is 25 for zirconia, v_0 is the crack velocity, c_0 and c_f are the initial and final radial crack size, and β is a crack geometry coefficient[12,15,16].

By incorporating the actual measurements of Young's modulus (obtained from the nanoindentation measurements) into the finite element simulations, an expression was obtained for the time-dependent stress $\sigma(t)$. The critical load vs loading rate measured by the Hertzian contact experiment above was then used to fit the value of D. Since D is only related to material properties and geometry, it should be consistent for different loading rates. Therefore, with D known, Eq. (2) was integrated to obtain the rupture time t_R and then the critical load P_c.

4. Results and discussion

4.1. Microstructure of fabricated dental multilayers

The fabricated dental multilayer was a sandwich structure with a soft composite substrate, a hard ceramic top layer and several layers of nanocomposite material in between. The resulting samples had a diameter of ~9 mm and a thickness of ~5 mm. It was cut open horizontally, polished and examined under an optical microscope, (National Optical DC-128 digital microscope, Microscope World, Carlsbad, CA) and by scanning electron microscopy (SEM) using an FEI Quanta™ 200 FEG Environmental-SEM instrument (FEI Company, Hillsboro, OR). The images of the cross section of the fabricated structure are presented in Fig. 7. The total thickness of the FGM multilayer was ~500 μm.

4.2. Young's moduli of fabricated FGM

Images of the typical indents in the images obtained from the scans of the tested surfaces are presented in Fig. 8a–c for the substrate of Z100 restoration, the FGM and the top zirconia ceramic layer, respectively. The Z100 substrate was found to have a modulus of ~20 GPa, while the top zirconia ceramic layer had a modulus >200 GPa. The measurements suggest an almost sinusoidal variation in Young's modulus across the 500-μm-thick FGM. It is also important to note the variations in Young's moduli for each of the data points that represented the average values and ranges ob-
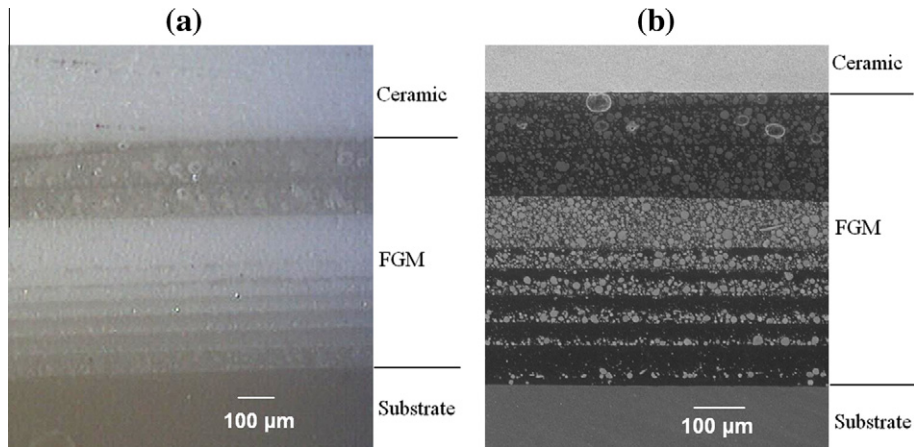
Fig. 7. Images of fabricated FGM structure cross section: (a) optical image; (b) SEM image.
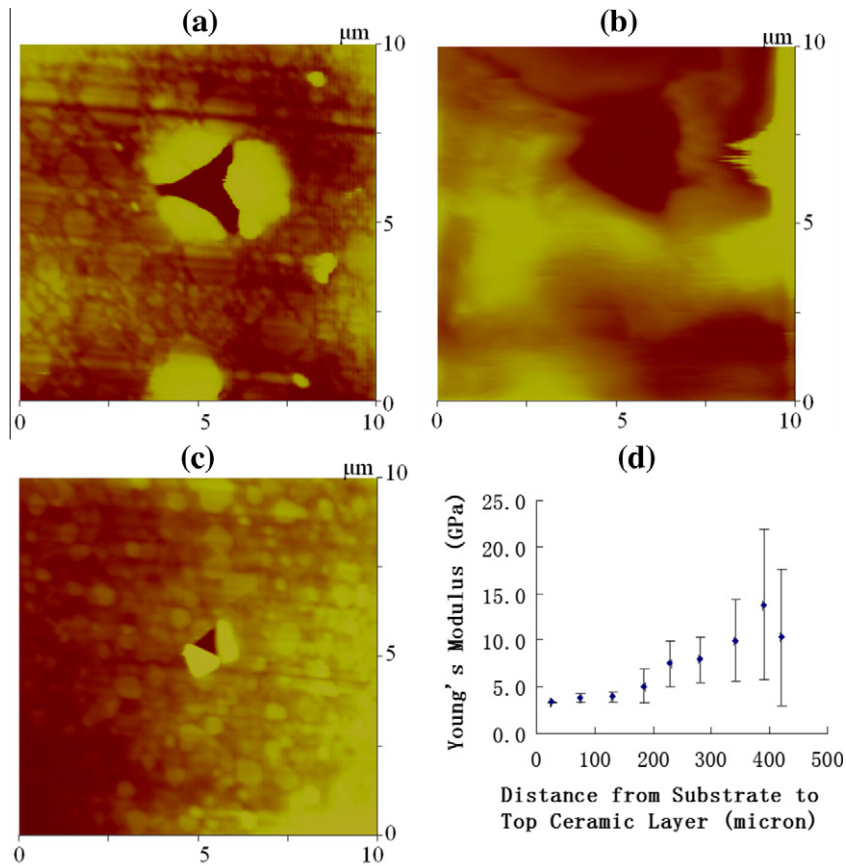

Fig. 8. Nanoindentation measurement results of the fabricated FGM Structure. (a) A typical image after the test on the substrate. (b) A typical image after the test on the FGM layer. (c) A typical image after the test on the top ceramic layer. (d) Distribution of Young's moduli across the FGM layer.

tained from three to six measurements. The variabilities in the Young's moduli are attributed partly to the clustering and non-uniform particle distributions that were observed in the optical microscopy images presented in Fig. 7. The images in Fig. 7 show the graded composite layers across the FGM region.

The Young's modulus of the Z100 substrate mimics the Young's modulus of the remaining dentin in natural teeth. Similarly, the dimension of the foundation has been chosen to mimic the dimension of remaining dentin in natural teeth. Hence, the compliance of the foundation should be similar to that of the remaining dentin in natural teeth. Also, when the thickness of the foundation is beyond its current thickness of 4 mm, the thickness of the foundation does

not have significant effects on the stress distribution at the bottom of the top ceramic layer.

4.3. Cracking modes and critical loads

Following the onset of pop-in, radial cracks were observed in the optical microscope. These were sometimes even visible with the naked eye. The tested samples were also cut open horizontally and examined under an optical microscope, (National Optical DC-128 digital microscope, Microscope World, Carlsbad, CA). Fig. 9 shows a typical subsurface radial crack observed in the ceramic top layer. Evidence of the interfacial cracking (between the top zir-
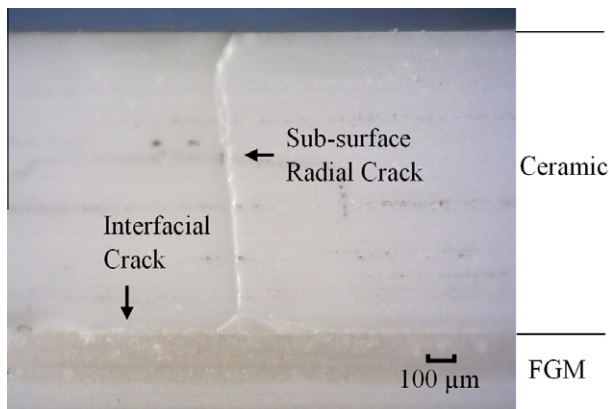
Fig. 9. Optical image of structure cross section after Hertzian contact test.

conia ceramic layer and the FGM layer) is also apparent in this image (Fig. 9). The current results, therefore, suggest that pop-in was associated with radial crack propagation into the top zirconia ceramic layer, along with partial interfacial cracking between the top zirconia ceramic layer and the FGM.

The critical loads obtained for the FGM structures are presented under Hertzian contact loading at different loading rates in Fig. 10. For each loading rate, between three and five samples were tested. The critical loads increased with increasing loading rates. For any given loading rate, the critical loads obtained for the FGM structures were greater than those obtained for the conventional non-FGM flat layered structures [17]. The differences were greater for slower loading rates than they were for faster loading rates. These suggest a loading rate dependence of the layer properties beyond those considered in this paper.

The predictions of the critical load were made by inputting the stresses obtained from FEM simulation into the SCG model. The predicted critical loads are plotted as hollow dots in Fig. 10. The time- and load-independent quantity D was fitted by the experimental results at the minimum loading rate. The estimated value D was then substituted into Eq. (2) to obtain the critical time t_R, which was used to estimate the critical load P_c from $t_R\dot{P}$. The results show clearly that the predictions from the SCG model were comparable with those obtained from the experiments on the FGM structure.

4.4. Implications

The current results suggest that the model bio-inspired FGM structures explored in this study could be used to engineer signif-
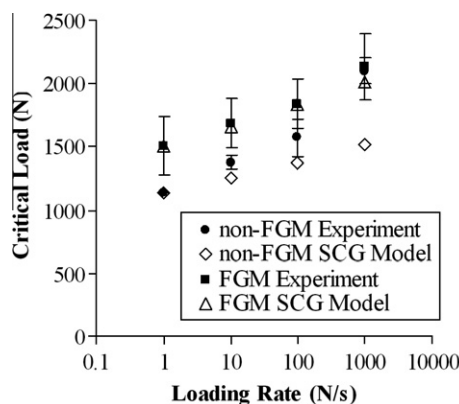

Fig. 10. Critical loads under different loading rates tested by Hertzian contact experiments and predicted by the SCG model. The experimental results for non-FGM structures are from Ref. [17].

icant improvements (∼20–40%) in the critical loads of dental multilayers. Such FGM structures could be fabricated using layering methods that spread nanocomposite layers across the regions between the top ceramic layer and the "dentin-like" Z100 composite layer. However, there is a need to develop more controlled nanocomposite layers across the FGM interlayers.

In any case, it is possible to envisage the development of functionally graded tapes, which could be integrated into the development of adhesive layers that can be used to attach ceramic crowns to "dentin-like" foundation layers. Such layered structures could be produced using nanocomposite layers that are similar to those examined in this study. They can also be produced using infiltration techniques [18] and a range of other methods [19] that are available for the processing of bio-inspired FGM. Further work is clearly needed to explore these possibilities. Basic studies of contact-induced failure are also needed to explore the effects of cyclic loading and environments that are relevant to occlusal contact. These are clearly some the challenges for future work.

5. Conclusions

This paper presented the results of a combined experimental and theoretical/computational study of the effects of layer architecture on the contact-induced fracture of bio-inspired, functionally graded, dental multilayers. The salient conclusions arising from this study are summarized below.

1. Finite element simulation of possible FGM architectures and conventional flat layered dental multilayers suggest that the FGM structures reduce the stresses in the top zirconia ceramic crowns. Greater reductions in the stresses in the ceramic crowns were observed when the gradients in the moduli of the FGM were higher near the ceramic layer.
2. The actual FGM structures fabricated using nanocomposite layers of epoxy/ceramic mixtures had ∼20–40% higher critical pop-in loads than flat conventional dental multilayers without FGM. The measured pop-in loads obtained at different loading rates (that are relevant to occlusal activity in the oral cavity) were also found to be comparable with predictions from a SCG model.
3. The current results suggest that bio-inspired, functionally graded, dental multilayers can be fabricated and incorporated into "tape" structures that can be used to reduce the top layer stresses in dental ceramic restorations. Further work is clearly needed to assess the clinical performance of such structures under cyclic loading conditions and environmental exposure relevant to occlusal conditions.

Appendix A. Figures with essential colour discrimination

Certain figures in this article, particularly Figs. 1, 2, 5–9, are difficult to interpret in black and white. The full colour images can be found in the on-line version, at http://dx.doi.org/10.1016/j.actbio.2012.08.034.

References

[1] Rekow D, Thompson VP. Engineering long term clinical success of advanced ceramic prostheses. J Mater Sci: Mater Med 2007;18:47–56.

[2] Burke FJT, Fleming GJP, Nathanson D, Marquis PM. Are adhesive technologies needed to support ceramics? An assessment of the current evidence. J Adhes Dent 2002;4:7–22.

[3] Malament KA, Socransky SS. Survival of Dicor glass–ceramic dental restorations over 14 years: Part I. Survival of Dicor complete coverage restorations and effect of internal surface acid etching, tooth position, gender, and age. J Prosthet Dent 1999;81:23–32.

[4] Shrotriya P, Wang R, Katsube N, Seghi R, Soboyejo WO. Contact damage in model dental multilayers: an investigation of the influence of indenter size. J Mater Sci: Mater Med 2003;14:17–26.

[5] Huang M, Wang R, Thompson V, Rekow D, Soboyejo WO. Bioinspired design of dental multilayers. J Mater Sci: Mater Med 2007;18:57–64.

[6] Kelly JR. Ceramics in restorative and prosthetic dentistry. Annu Rev Mater Sci 1997;27:443–68.

[7] Marshall GW, Balooch M, Gallagher RR, Gansky SA, Marshall SJ. Mechanical properties of the dentinoenamel junction: AFM studies of nanohardness, elastic modulus, and fracture. J Biomed Mater Res 2001;54:87–95.

[8] Niu X, Rahbar N, Farias S, Soboyejo W. Bio-inspired design of dental multilayers: experiments and model. J Mech Behav Biomed Mater 2009;2: 596–602.

[9] Rahbar N, Soboyejo WO. Design of functionally graded dental multilayers. Fatigue Fract Eng M 2011;34:887–97.

[10] Kelly JR. Clinically relevant approach to failure testing of all-ceramic restorations. J Prosthet Dent 1999;81:652–61.

[11] Bourne MC. Compression rates in the mouth. J Texture Stud 1977;8:373–6.

[12] Lee C-S, Kim DK, Sanchez J, Pedro M, Antonia P, Lawn BR. Rate effects in critical loads for radial cracking in ceramic coatings. J Am Ceram Soc 2002;24: 2019–24.

[13] Niu X, Soboyejo W. Effects of loading rate on the deformation and cracking of dental multilayers: experiments and models. J Mater Res 2011;21:970–5.

[14] Zhang Y, Lawn BR, Rekow ED, Thompson VP. Effect of sandblasting on the long-term performance of dental ceramics. J Biomed Mater Res B: Appl Biomater 2004;71:381–6.

[15] Dabbs TP, Lawn BR, Kelly PL. A dynamic fatigue study of soda-lime silicate and borosilicate glasses using small scale indentation flaws. Phys Chem Glasses 1982;23:58–66.

[16] Huang M, Niu X, Soboyejo WO. Creep induced rate effects on radial cracks in multilayered structures. J Mater Sci: Mater Med. 2007;18:65–9.

[17] Niu X, Yang Y, Soboyejo W. Contact deformation and cracking of zirconia/cement/foundation dental multilayers. Mater Sci Eng A: Struct Mater 2008;485:517–23.

[18] Zhang Y, Ma L. Optimization of ceramic strength using elastic gradients. Acta Mater 2009;57:2721–9.

[19] Ilschner B. Processing–microstructure–property relationships in graded materials. J Mech Phys Solids 1996;44:647–56.